Links between through-bond interactions and assembly structure in simple piperidones†

Ling Yuan,[a] Bobby G. Sumpter,[b] Khalil A. Abboud[a] and Ronald K. Castellano*[a]

Received (in Gainesville, FL, USA) 28th May 2008, Accepted 12th June 2008
First published as an Advance Article on the web 16th July 2008
DOI: 10.1039/b808818g

3,5-Disubstituted piperidones provide an opportunity to explore donor–acceptor through-bond interactions in the context of molecular and supramolecular structure. The crystal structure of *cis*-3,5-dibenzyl-1-phenylpiperidin-4-one **3** is disordered and the lattice accommodates a ~3 : 1 ratio of the *N*-Ph equatorial (**3**-*eq*) and *N*-Ph axial (**3**-*ax*) epimers, based on refined values of occupancy factors. The fortuitous result allows a side-by-side comparison of the two configurations with respect to their donor–acceptor through-bond interactions. The energy difference between **3**-*ax* and **3**-*eq* (ΔE_{ax-eq}) has been evaluated in the gas phase using extensive first principles calculations, and for many levels of theory this difference parallels the experimentally-observed configurational ratio in the solid state (where the epimers share nearly identical packing environments). The calculations further show a difference in the through-bond stabilization for **3**-*ax* and **3**-*eq*, with larger contributions for **3**-*ax*. Natural bond order (NBO) analysis quantifies the delocalization of the donor nitrogen lone pair into the adjacent carbon–carbon bonds and carbonyl acceptor for the **3**-*ax* epimer. The work concludes that molecular-level structural perturbations that arise from or otherwise influence through-bond donor–acceptor interactions have consequences on solid-state and supramolecular assembly structure.

Introduction

The rigid covalent framework of β-aminoketones **1**, 1-aza-adamantanetriones[1] (AATs), fosters efficient through-bond[2] (hyperconjugative[3]) communication between the bridgehead nitrogen donor and three carbonyl acceptors. Consequences at the molecular level include changes in bond lengths and angles within the donor–σ-acceptor core, emergence of a new absorption band in the UV/Vis spectrum (the "σ-coupled transition"[4]), and dramatic changes in chemical reactivity.[1b] Functionalized AATs have appeared as vehicles to explore "strong" through-bond interactions "beyond-the-molecule"[5] for the first time in the context of solution-phase self-assembly.[6] Both **1a** and **1b** (Fig. 1), for example, show extensive aggregation in organic solvents that is manifested, at low concentrations (*ca.* 0.5% by weight for **1a** and **1b**), in organogelation.[6a,b] The macromolecular properties respond to the chemical substituents on the core in ways that implicate its unique donor–acceptor configuration,[6c] and recent theoretical studies find that an unprecedented electronic structure emerges for 1-D arrangements of the molecules in the gas phase.[7]

The interplay between self-assembly and through-bond interactions emerging for the AATs encourages studies of even simpler systems wherein σ-coupled donor–acceptor interactions might be linked to a supramolecular event or structure. Considered here are piperidones **2** and **3** (Fig. 1), functional fragments of **1a**, for which the configuration at nitrogen that optimizes donor–acceptor through-bond interactions is not fixed. The equilibrium that describes interconversion between the axial (*ax*) and equatorial (*eq*) forms of **2** is shown as an

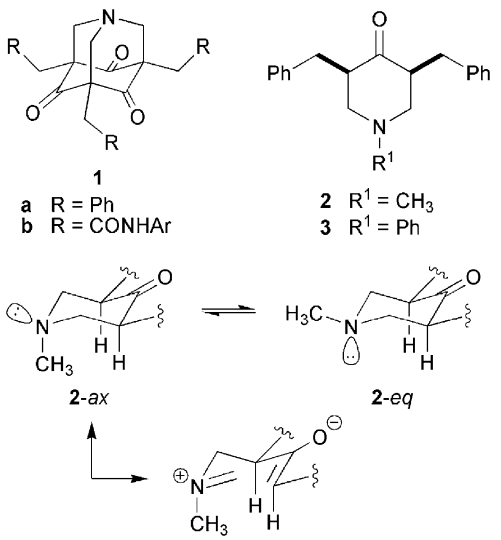

Fig. 1 Substituted 1-aza-adamantanetriones **1** and their *cis*-3,5-dibenzylpiperidin-4-one counterparts **2** and **3**.

[a] *Department of Chemistry, University of Florida, P.O. Box 117200, Gainesville, FL 32611-7200, USA. E-mail: castellano@chem.ufl.edu; Fax: +01 352 846 0296; Tel: +01 352 392 2752*
[b] *Computer Science and Mathematics Division and Center for Nanophase Materials Sciences, Oak Ridge National Laboratory, Oak Ridge, TN 37831, USA*

† Electronic supplementary information (ESI) available: Cartesian coordinates and energies for all calculated structures. CCDC reference numbers 686114 (**2**) and 686115 (**3**). For ESI and crystallographic data in CIF or other electronic format see DOI: 10.1039/b808818g

example. It is established from both experimental and theoretical work that the *axial* configuration with respect to the nitrogen substituent is required to optimize (''turn on'', depicted graphically by a no-bond resonance structure) donor–acceptor through-bond interactions in cyclic β-aminoketones and related structures.[4,8] Given that these types of molecules (a) may hold potential for electronic applications[7,9] and (b) show relationships between their bulk properties and unique electronic configurations, elucidating the relationship between the *ax* : *eq* ratio and molecular/supramolecular structure is important.

The *cis*-3,5-dibenzyl substituents of **2** and **3** (Fig. 1) allow the molecules to be easily crystallized. The structure of **3** is disordered, but can be suitably refined based on a two-site occupancy that corresponds to the axial (**3**-*ax*) and equatorial (**3**-*eq*) nitrogen configurations (~3 : 1 *eq* : *ax*). The result is fortuitous in that it places the epimers in similar solid-state environments and encourages a side-by-side analysis of their energies and electronic structures; a line of investigation typically precluded and with results that are obscured by ''packing effects''. Through high-level calculations that include natural bond order analysis, to date sparsely performed on similar donor–σ-acceptor systems,[10] a surprising relative stability for **3**-*ax* is revealed, in part a consequence of hyperconjugative interactions. Several computational approaches are explored, all that treat electron correlation well, and several find gas-phase energy differences between **3**-*ax* and **3**-*eq* that on-average parallel the solid-state results. Further revealed, by comparison of **2** to **3** and several other model compounds, is that simple functionalization of piperidones can substantially bias the *ax* : *eq* ratio. This combined experimental and theoretical study shows that molecular-level structural changes linked to through-bond interactions can have consequences on assembly and therefore, bulk properties.

Results and discussion

Synthesis of *cis*-3,5-dibenzylpiperidin-4-one derivatives

Synthesis of **2** and **3** follows classical condensation chemistry (Scheme 1). Starting piperidones **4** were commercially available (**4a**) or readily obtained (**4b**[11]). Standard base-catalyzed solution-phase conditions (NaOH, EtOH) were found to work best to effect the aldol cross-condensation between *N*-methylpiperidone **4a** and benzaldehyde to give dibenzylidene derivative **5a** (in 54% isolated yield), echoing observations in the literature.[12] Other dibenzylidenes, including **5b**, were only prepared in comparable yield (~50%) using solvent-free conditions and ytterbium triflate catalysis.[13] Both **5a** and **5b** were isolated in the expected *E*,*E* configuration.[12b] Hydrogenation of **5a** and **5b** in the presence of catalytic palladium on carbon then provided dibenzylpiperidones **2** and **3**, respectively, with the *cis* relative stereochemistry of the benzyl side chains (>80% d.e.). Initial hydrogenation attempts using the Adams platinum oxide catalyst as described for similar systems by McElvain[12a] unfortunately also resulted in facile reduction of the carbonyl group to the corresponding secondary alcohol. Palladium on carbon worked quite efficiently as a substitute catalyst provided that high hydrogen pressures were

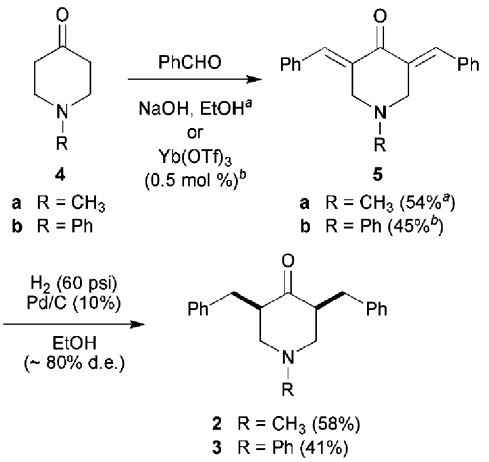

Scheme 1 Synthesis of *cis*-3,5-dibenzylpiperidin-4-one derivatives.

used (*i.e.*, 60 psi).[14] Worth noting, no significant epimerization at positions C(3) or C(5) has been detected in these molecules after even prolonged storage at room temperature in the laboratory.[15]

X-Ray crystal structure of 2: general features and packing

Fig. 2 shows the X-ray crystal structure of **2**. Selected bond lengths and angles are presented in Tables 1 and 2. The two benzyl groups are *cis* diequatorial (Fig. 2(a)) and the piperidone ring adopts a standard chair conformation. The

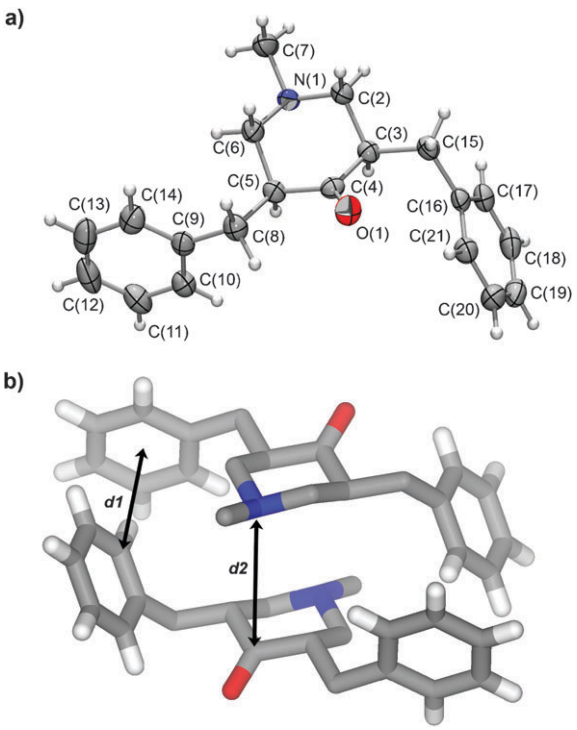

Fig. 2 The X-ray crystal structure of **2**: (a) An ORTEP diagram of **2**. Displacement ellipsoids are drawn at the 50% probability level; (b) close-packed dimers with near perfect edge-to-face interactions and dipolar core alignment ($d1$ = 3.76 Å; $d2$ = 3.95 Å). Atom colors: blue N, red O, white H.

Table 1 Selected bond lengths (Å) for **2**, **3**-*eq*, and **3**-*ax*[a]

Bond	**2**	**3**-*eq*	**3**-*ax*[b]
N(1)–C(2)	1.4611(13)	1.4755(18)	1.457(7)
N(1)–C(6)	1.4604(13)	1.4524(17)	1.407(6)
N(1)–C(7)	1.4617(13)	1.4340(19)	1.462(6)
C(2)–C(3)	1.5359(15)	1.519(2)	1.487(9)
C(5)–C(6)	1.5312(14)	1.545(2)	1.556(8)
C(3)–C(4)	1.5100(14)	1.521(3)	1.517(11)
C(4)–C(5)	1.5096(15)	1.510(3)	1.504(11)
C(4)–O(1)	1.2178(12)	1.209(3)	1.191(14)

[a] Standard deviations are shown in parentheses. Additional crystallographic details are provided in the Experimental section. [b] Corresponding atom labels are primed (see Fig. 3(b)).

Table 2 Selected bond angles (°) for **2**, **3**-*eq*, and **3**-*ax*[a]

Angle	**2**	**3**-*eq*	**3**-*ax*[b]
C(2)–N(1)–C(6)	110.09(9)	110.33(11)	111.6(4)
C(2)–N(1)–C(7)	111.35(8)	111.40(11)	119.5(4)
C(6)–N(1)–C(7)	110.65(9)	116.19(12)	116.4(4)
$\sum_{CNC}$	332.1	337.9	347.5
N(1)–C(7)–C(22)	—	123.81(15)	116.2(4)
N(1)–C(7)–C(26)	—	117.55(18)	123.6(4)
C(3)–C(2)–N(1)	110.51(9)	112.57(13)	115.4(5)
C(5)–C(6)–N(1)	111.36(8)	109.89(11)	113.6(4)
C(4)–C(3)–C(2)	107.70(8)	109.03(15)	112.4(6)
C(4)–C(5)–C(6)	108.47(9)	108.37(15)	109.3(5)
C(4)–C(3)–C(15)	114.14(9)	113.02(15)	111.2(5)
C(4)–C(5)–C(8)	113.36(9)	110.90(14)	108.6(6)
C(3)–C(4)–C(5)	113.84(9)	115.62(17)	114.2(7)
C(3)–C(4)–O(1)	123.48(10)	121.3(2)	121.1(10)
C(5)–C(4)–O(1)	122.62(10)	123.0(2)	123.9(10)

[a] Standard deviations are shown in parentheses. Additional crystallographic details are provided in the experimental section. [b] Corresponding atom labels are primed (see Fig. 3(b)).

equatorial *N*-CH_3 epimer is observed (**2**-*eq*), a configuration at nitrogen that allows individual molecules to form closely-packed dimers (Fig. 2(b)). Several key interactions highlight this assembly: near perfect edge-to-face aromatic interactions are found with *d*1 (distance between the ring carbon C(17) and neighboring ring centroid) = 3.76 Å and an angle between the aromatic planes of 89.7°; this geometry optimizes the electrostatic interactions between the protons on the ring edge and the π-electron density on the ring face.[16] Stabilizing dipolar (electrostatic) interactions come through an antiparallel alignment of the cores; more subtle electrostatic matching between the piperidone nitrogens and carbonyl carbons is also evident (Fig. 2(b); *d*2 = 3.95 Å). The extended crystal packing for **2** (not shown) features additional edge-to-face aromatic interactions between the rings of the dimeric units.

X-Ray crystal structure of 3: general features and packing

The X-ray structure of *N*-phenylpiperidone **3** at 173 K is disordered; both the equatorial (**3**-*eq*) and axial (**3**-*ax*) epimers of the compound are accommodated in the crystal lattice, in a ~3 : 1 ratio (76 ± 1% **3**-*eq*; 24 ± 1% **3**-*ax*) based on refined values of occupancy factors. Configurational disorder at nitrogen has been identified and studied before in other *N*-heterocycles in the solid state,[10b,17] but not, based on our searching, with cyclic β-aminoketones. It provides a rare opportunity here to compare the two epimers in similar solid state environments (*vide infra*).

The AAT systems **1** (Fig. 1) are unusual in that they show pronounced bond length changes consistent with hyperconjugative interactions; for example, a slight shortening of the N(1)–C(2) and N(1)–C(6) bonds (to 1.45 Å), and a lengthening of the central C(2)–C(3) and C(5)–C(6) bonds (to 1.59 Å).[1b] Fig. 3(a) and (b) show the two nitrogen epimers of **3** as they are found in the crystal. Tables 2 and 3 then summarize the key bond angles and distances, respectively. The stereoelectronic requirements for optimized through-bond interactions (Fig. 1) predict that the piperidone ring bond lengths of **2** and **3**-*eq* might be both similar and "normal" when compared to **3**-*ax*. Such an analysis is unfortunately precluded here by the disorder of **3**, particularly with respect to **3**-*ax*, the minor of the two epimers. Evaluation of subtle bond angle changes with respect to through-bond interactions could be equivalently risky. High-level calculations using the crystal structures as a starting point provide a better way to probe these stereoelectronic effects (*vide infra*).

The two epimers of **3** do share similar packing environments (Fig. 3(c) and (d)); the aromatic rings in each experience a number of readily characterizable contacts. The *N*-Ph groups show close edge-to-face interactions with neighboring benzyl substituents, defined here by the C(24)-centroid distances (*d*1 = 3.70 Å; *d*3 = 4.13 Å). The angle between the aromatic planes is also around the ideal 90° (**3**-*eq* = 85.6°; **3**-*ax* = 84.3°). Slipped (offset) face-to-face interactions are found that can be defined by the ring centroid to ring centroid distance (*d*2 = 3.99 Å; *d*4 = 4.15 Å). The distance between the ring planes is 3.60 Å for **3**-*eq* and a short 3.24 Å for **3**-*ax* in this configuration. The packing forces certainly influence the pliable twist angle about the N(1)–C(7) bond (calculated from the angle between the rms planes defined by atoms C(4)–N(1)–C(7) and atoms C(7)–C(23)–C(25)) that is 35.2° in **3**-*eq* and 33.7° in **3**-*ax*.

Not necessarily decoupled from the packing and important for consideration of through-bond interactions is the pyramidalization at N(1), analyzed thoughtfully in a variety of related systems.[8,10b] As a baseline, the nitrogen of **2** is, as expected, strongly pyramidalized based on the sum of the C–N–C bond angles ($\sum_{CNC}$ = 332°). The nitrogen is slightly flattened in **3**-*eq* ($\sum_{CNC}$ = 338°) and more significantly flattened in **3**-*ax* ($\sum_{CNC}$ = 348°). The latter presumably reflects conjugation between the nitrogen and phenyl ring in the axial epimer that also minimizes steric repulsion; however, the N(1)–C(7) twist angles are nearly the same in **3**-*ax* and **3**-*eq* (*vide supra*).

Weaker and longer aromatic contacts (*e.g.* edge-to-face involving the benzyl groups) then define the packing structures (Fig. 3(e) and (f)). Unlike the structure of **2** in which the monomers are oriented into antiparallel dimers, **3** forms abutting one-dimensional stacks that feature the carbonyl groups all pointing in the same direction with respect to the column axis. The macrodipole created within one pair of stacks is cancelled by a neighboring pair. The intracolumnar nitrogen-to-nitrogen distance is 5.5 Å, a distance nearly identical to that postulated for 1-D stacks of **1**.[6c,7] Also observed are C–H···O interactions[18] between the piperidone carbonyl

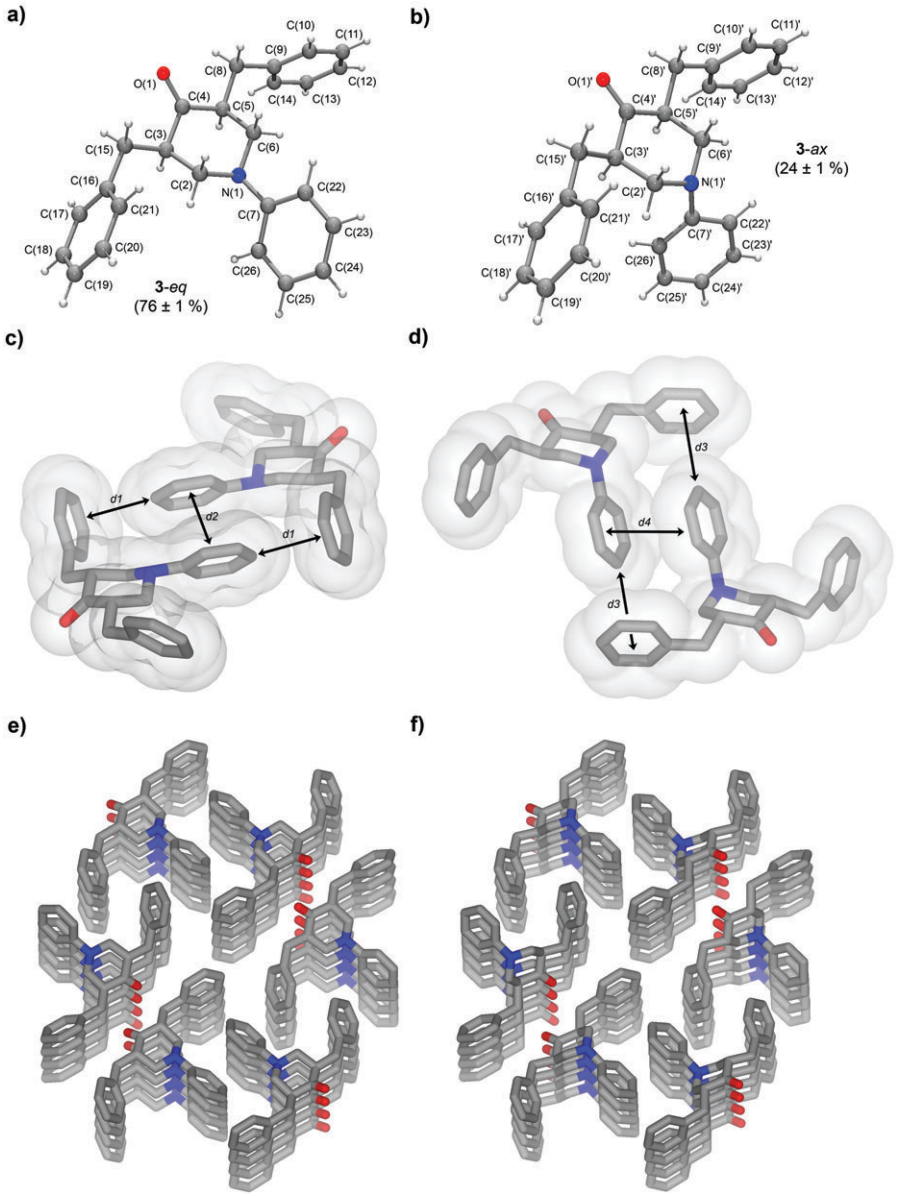

Fig. 3 The X-ray crystal structure of **3** is disordered and refined based on a 76% occupancy of **3**-*eq* (a) and a 24% occupancy of **3**-*ax* (b). The local packing environments of **3**-*eq* (c) and **3**-*ax* (d) are similar with respect to their aromatic contacts ($d1$ = 3.70 Å; $d2$ = 3.99 Å; $d3$ = 4.13 Å; $d4$ = 4.15 Å). The molecules are further organized into 1-D columns with a nitrogen-to-nitrogen intracolumnar distance of 5.5 Å (e and f). Atom colors: blue N, red O, white H. The van der Waals surfaces shown were generated in Discovery Studio Visualizer 2.0 (Accelrys Software, Inc.).

oxygens and both the benzylic CH_2 hydrogens and the benzyl aromatic C–H hydrogens ($d_{C\cdots O}$ = 3.5 Å).

The sensitivity of the **3**-*eq* : **3**-*ax* ratio to temperature and crystal preparation has been investigated. A second X-ray quality crystal was obtained from a different synthetic batch of **3**; the epimer ratio at 173 K (69 ± 1% **3**-*eq*; 31 ± 1% **3**-*ax*) appeared similar to first sample where again the axial epimer was the minor component, but well represented. The disorder in this sample showed no dependence on temperature based on data collection at 297 K (68 ± 1% **3**-*eq*; 32 ± 1% **3**-*ax*) and 123 K (69 ± 1% **3**-*eq*; 31 ± 1% **3**-*ax*). The conclusion is that the epimers do not equilibrate in this temperature range in the solid state—static disorder—although the energy barrier for doing so in solution is small (*vide infra*).

Properties in solution

Conformation and relative stereochemistry. ^{1}H NMR experiments corroborate the solid-state conformations and relative stereochemistry of **2** and **3** in solution. Provided in Table 3 are the ^{1}H NMR chemical shifts and $^3J_{H,H}$ (vicinal) coupling constants for the compounds. From the $^3J_{a,c}$ and $^3J_{b,c}$ values for **2** (in $CDCl_3$) and **3** (in toluene-d_8) it is clear that the benzyl groups at positions C(3) and C(5) are *cis* diequatorial and that the molecules adopt chair conformations. Taking **2** as an example, the $^3J_{c,d}$ (3.5 Hz) and $^3J_{b,c}$ (8.8 Hz) coupling constants support the solid-state benzyl substituent conformation wherein the CH_2Ph group is staggered with respect to the piperidine ring and H_c. For **3** in $CDCl_3$, H_a and H_b are deshielded by the neighboring phenyl ring. The difference in

Table 3 ^{1}H NMR data for compounds **2** and **3**[a]

	2	**3**	**3**[b]
H_a (δ, ppm)	2.98	3.90	3.66
H_b (δ, ppm)	2.04	2.88	2.46
H_c (δ, ppm)	2.93	2.90	2.54
H_d (δ, ppm)	3.25	3.31	3.23
H_e (δ, ppm)	2.40	2.49	2.34
N-CH_3 (δ, ppm)	2.22[c] (1.74[d], 2.49[e])	—	—
ortho-CH (*N*-Ph) (δ, ppm)	—	6.62	6.49
$J_{a,c}$/Hz	5.1	—	4.8
$J_{b,c}$/Hz	11.1	—	12.1
$J_{c,d}$/Hz	3.5	—	4.5
$J_{c,e}$/Hz	8.8	—	8.4

[a] All data recorded in $CDCl_3$ at 21 °C unless otherwise specified and chemical shifts are reported relative to TMS. [b] In toluene-d_8. [c] The *N*-CH_3 protons of 1-methyl*piperidine* appear at δ 2.24, 2.23, and 2.10 ppm in C_6D_6, $CDCl_3$, and DMSO-d_6, respectively. [d] In C_6D_6. [e] In DMSO-d_6.

chemical shift between H_a and H_b speaks, in part, to the on average positioning of the phenyl substituent with respect to the symmetry plane of the piperidone ring; here the phenyl group is likely twisted to some extent about the *N*-Ph bond and H_a experiences a larger ring current effect.[17e,19]

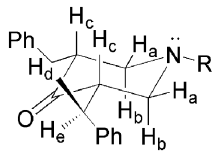

2 R = CH_3
3 R = Ph

Solvent dependence of chemical shifts. Some donor–σ-acceptor molecules show substantial chemical shift responses to solvent polarity, noted previously for **1a**.[6a] The *N*-CH_3 group of compound **2** is a sensitive probe of this behavior. Considerable downfield shifts ($\Delta\delta$ = 0.75) are found for **2** (Table 3) upon moving from C_6D_6 (ε = 2.3) to DMSO-d_6 (ε = 47),[20] consistent with stabilization of the core dipole (polarization effects) and the nitrogen developing an increasing partial positive charge, while the opposite trend is found for simple 1-methylpiperidine ($\Delta\delta$ = −0.14) that lacks an acceptor group. Whether this behavior is coupled with variation of the equilibrium **2**-*eq* : **2**-*ax* ratio is not known. For **3**, the protons are in general more deshielded in the more polar $CDCl_3$ *vs.* toluene-d_8. Also interesting is that the chemical shift difference between H_a and H_b increases slightly in **3** (*vs.* **2**), possibly related to a conformational change with respect to the *N*-Ph substituent.

Nitrogen configuration. Piperidones **2** and **3** show no substantial change in their ^{1}H NMR spectra in $CDCl_3$ from room temperature to −55 °C; the nitrogen inversion barrier is simply too low to be readily measured. The barriers are likely similar to that of *N*-methylpiperidine ($\Delta G^{\ddagger} \sim$ 6–9 kcal mol^{-1}),[21] even lower for **3** given that the transition state for nitrogen inversion is stabilized by conjugation with the phenyl ring. Additionally, the UV/Vis spectra of the molecules in solution (CH_3CN) show no evidence of the so-called "σ-coupled transition" (λ_{max} 220–260 nm).[4] For **2** this is presumably due to the methyl group preferentially adopting the equatorial position (*vide infra*);[8a–d] for **3**, this relevant (and weak; $\varepsilon \sim$ 500–2500 M^{-1} cm^{-1}) absorption is otherwise masked by the stronger absorption bands of the *N*-Ph chromophore.

Discussion and theoretical analysis

Configurational preferences at nitrogen in the solid state

Unlike the solid-state structures of the AATs (**1**), hallmark (and more subtle) intramolecular structural changes as a consequence of through-bond interactions are difficult to assess in **3** due, in part, to crystallographic disorder. These include perturbed bond lengths and angles, and pyramidalization effects at nitrogen or the carbon of the carbonyl.[1b,8f,h] Still intriguing is that **3**-*ax* is highly represented in the solid state, an appearance not obviously linked to a much differently packed structure. Translating solid state conformer (or epimer) ratios into meaningful energetic differences ranges from risky to inappropriate; only in certain cases[22] can these connections be considered. In our case, the co-representation of **3**-*ax* and **3**-*eq* provides such an opportunity.

The notion that through-bond donor–acceptor effects might be significant enough to bias solution-phase and solid-state conformations is credited to Verhoeven and co-workers who have performed numerous seminal studies with 1,1′-dicyanoethylene-derivatized piperidones and tropinones.[8f,i,j] Related findings have been reported by Jenneskens and co-workers.[8h] On the other hand, Ogawa and co-workers have shown that crystal packing effects can significantly influence the nitrogen configuration of various *N*-phenylpiperidines; there are certainly cases where the higher-energy epimers of such compounds may selectively crystallize.[10b] The observation is a universal one.[23] The disorder that defines **3**-*ax* and **3**-*eq* represents the first case for simple piperidones where the packing argument is at least partially abated.

To be complete, we have performed a Cambridge Structural Database search of *N*-alkyl and *N*-arylpiperidines/-ones. The query was restricted to include only organic structures with *R* factors better than 0.05; also eliminated were piperidines/-ones that (a) were not in chair conformations (*e.g.*, those with fused ring structures or vinylic C(3)/C(5) carbons) and (b) bore

Table 4 Energy difference between the axial (*ax*) and equatorial (*eq*) epimers for molecules **2**, **3**, **6–11** at various levels of theory[a]

Level of theory	**6**	**7**	**8**	**9**	**10**	**11**	**2**	**3**
B3LYP/6-31G*	3.4[c]	—	1.5[c]	—	—	—	—	0.18
MP2/6-31G*	3.32[b]	2.36[b]	—	—	—	—	—	–2.16
MP2/6-311++G**	3.37	2.25	–0.012	–0.997	–0.15	–1.99	–0.24	–3.31

[a] Reported as *E*(axial) − *E*(equatorial); a negative number means that the axial configuration is more stable in the gas phase. [b] See ref. 10*a*. [c] See ref. 10*b*.

substituents at C(2) or C(6)). Of the 280 or so piperidine candidates, there are only about a dozen *N*-C(sp^2) derivatives that are axially or pseudo-axially disposed (see, for example, CSD codes CEQXUS, EZOPAK, HUFROP, LUPVUN and VUCHIK). Most molecules of this type (*e.g.*, *N*-acylpiperidines) feature definitively sp^2-hybridized N atoms, a consequence of extensive π-conjugation between the nitrogen and its substituent. No axially-configured *N*-alkylpiperidines were identified. For the piperidones, only *two* *N*-alkyl (CSD codes: DIKVUP and FEKNUE) and no *N*-aryl derivatives were found; both of the former are in the *equatorial* configuration. On the basis of CSD searching, the appearance of **3**-*ax* is quite uncommon.

Configurational preferences at nitrogen in solution

Solution-phase values for the energy difference between the equatorial and axial configurations at nitrogen of *N*-methylpiperidine have been controversial, but most sources report a $\Delta G^\circ \sim 3$ kcal mol^{-1} in favor of the former.[21] The equilibrium constant is similar for *N*,*cis*-3,5-trimethylpiperidine ($\sim$3 kcal mol^{-1}), again in favor of the equatorial configuration, that is substituted similarly to the molecules discussed in this work.[24] Experimental measurements with the corresponding *N*-methylpiperidones, *N*-phenylpiperidines, and *N*-phenylpiperidones are comparatively scarce, although some aspects have been taken up computationally (*vide infra*). The phenyl group of *N*-phenylpiperidine, for example, is known to be preferentially equatorial in solution,[15,25] although this has not been rigorously quantified.

Theoretical studies

Little is known about the energetic differences between the *ax* and *eq* configurations in simple piperidones, particularly for *N*-Ph derivatives,[10b,26] despite the fact that these molecules lend themselves well to comprehensive high-level theory that can evaluate energy differences between conformers and interrogate their respective electronic structures.[10a] The molecules considered, in addition to **3**-*ax* and **3**-*eq*, are shown in Fig. 4 (and the results are provided in Tables 4 and 5). The series will first establish a baseline energy difference between *eq* and *ax* epimers when N is substituted with methyl (**6**, **10**) or phenyl (**8**, **11**), in the presence and absence of benzyl substituents at positions 3 and 5 of the piperidine ring. The energy differences (between *ax* and *eq*, ΔE_{ax-eq}) are then evaluated in the presence and absence of the acceptor (C=O); that is, when through-bond donor–acceptor interactions are "turned on" or "turned off."

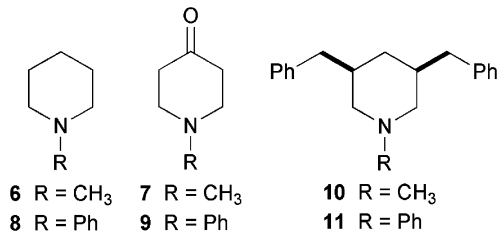

Fig. 4 Structures of molecules considered for computational studies (in addition to **3**-*ax* and **3**-*eq*).

Utilized here are levels of theory that treat electron correlation well, a prerequisite for considering hyperconjugative effects in such molecules (*vide infra*).[10a] These include MP2, CCSD, CCSD(T), CASSCF and DFT. The results, in terms of ΔE_{ax-eq}, report on electron correlation effects when compared to those obtained from simple Hartree–Fock (HF) theory that neglects electron–electron interactions. Even so, each non- or post-HF method treats electron correlation (and for DFT, electron exchange) differently; these subtleties are discussed in the computational methods section (*vide infra*). Beginning with the simplest piperidine case, **6**, the MP2/6-311++G** level predicts a 3.4 kcal mol^{-1} advantage for **6**-*eq* *vs.* **6**-*ax*, a value similar to that reported by DFT (B3LYP/6-31G*)[10b] and MP2/6-31G* calculations.[10a] Each of these values is close to the experimentally reported one.[21] This energy difference diminishes significantly, by 1.1 kcal mol^{-1}, upon introduction of the carbonyl acceptor (**7**) at the MP2/6-311G++** level. Brouwer and co-workers report a similar 1.0 kcal mol^{-1} decrease at the MP2/6-31G* level.[10a] A comparable axial stabilization is also observed for **8** *vs.* **9** (0.99 kcal mol^{-1}) and **11** *vs.* **3** (1.3 kcal mol^{-1}). The value is, however, reduced for **10** *vs.* **2** (<0.1 kcal mol^{-1}), and this may speak to a difference in the relative magnitude of stabilization between *N*-CH_3 and *N*-Ph in the 3,5-disubstituted derivatives. Finally, it is interesting to note for **3** (and to a lesser extent **8**) the quite different ΔE_{ax-eq} values between the DFT and MP2 methods. Given the consistency between the methods for **6**, some of this disparity likely arises from how they handle electron correlation (*vide infra*).

As first reported by Ogawa *et al.*,[10b] the phenyl substituent can, despite its size, better approach an axial positioning than a methyl group by maintaining some delocalization of the nitrogen lone pair into the ring.[23b] At the DFT level, this amounts to a reduction in the ΔE_{ax-eq} value by $\sim$1.9 kcal mol^{-1} for **8** *vs.* **6**. Our MP2 calculations give this difference as a larger $\sim$3.4 kcal mol^{-1} such that $E_{ax} \cong E_{eq}$ at this level. Similar energetic differences characterize **7** *vs.* **9** (3.2 kcal mol^{-1}), **10** *vs.* **11** (1.8 kcal mol^{-1}), and **2** *vs.* **3** (3.1 kcal mol^{-1}). Therefore, conversion of the *N*-CH_3 function to *N*-Ph results in a 1.8–3.4 kcal mol^{-1} swing in relative stability toward *ax*.

A surprising finding emerges related to 3,5-dibenzyl substitution of the piperidine ring, where a further energetic tilt toward *ax* is observed. The energy differences are: **6** *vs.* **10** (3.5 kcal mol^{-1}), **8** *vs.* **11** (2.0 kcal mol^{-1}), **7** *vs.* **2** (2.5 kcal mol^{-1}), and **9** *vs.* **3** (2.3 kcal mol^{-1}). Discussed earlier, there is virtually no difference in the *ax*-*eq* ratio between *N*-methylpiperidine and *N*,*cis*-3,5-trimethylpiperidine in solution. The result then implicates the π-systems of the phenyl groups as potentially important stabilizing groups. The combination of all of the effects—the carbonyl acceptor, 3,5-dibenzyl substitution, and *N*-Ph substitution—leads to a significant predicted stability advantage for **3**-*ax* at the MP2/6-311++G** level (3.3 kcal mol^{-1}). These structural modifications could be general ones to optimize through-bond interactions in simple piperidones.

Various levels of theory treat the energy differences between **3**-*ax* and **3**-*eq* differently (Table 5), and a systematic study is important for future computations that consider through-bond interactions in β-aminoketones or related molecules. The effects of electron correlation on ΔE_{ax-eq} is reinforced

Table 5 Energy difference between the axial (*ax*) and equatorial (*eq*) epimers (with respect to nitrogen configuration) for **3**-*ax* and **3**-*eq* at various levels of theory[a]

Basis	HF	MP2	CCSD	CCSD(T)	CASSCF (10,10)	LDA	PBE0	B3LYP
STO-3G	—	—	1.1	0.6	—	—	—	—
6-31G*	2.34	–2.16	—	—	3.0	–3.3	–0.57	0.18
6-31G**	2.26	–2.52	—	—	3.36, 2.3[b]	–3.4	–0.90	0.10
6-311G**	1.91	–2.45	—	—	—	–3.2	–0.08	0.36
6-311++G**	2.42	–3.31	—	—	—	—	—	—
cc-pvdz	2.31	–2.74	–0.36	–1.3	—	–3.1	–0.62	0.11
cc-pvtz	2.27	—	—	—	—	—	—	0.31

[a] Reported as *E*(axial) − *E*(equatorial) in kcal mol^{-1}; a negative number means that the axial configuration is more stable in the gas phase. [b] CASSCF using 12 orbitals (6 occupied and 6 unoccupied molecular orbitals) and 12 electrons.

by comparing results obtained from simple Hartree–Fock (HF) theory to those obtained with methods that treat correlation (such as MP2, CCSD, CI or DFT). HF predicts that **3**-*eq* is significantly more stable (by 1.9–2.4 kcal mol^{-1}) over a range of basis sets. Adding in the effects of dynamical electron correlation by implementing many body perturbation theory (MBPT) significantly predicts **3**-*ax* to be the most stable (*e.g.*, ΔE(MP2/cc-pvdz) = −2.74 kcal mol^{-1}). Similarly, DFT methods (LDA and PBE0) predict **3**-*ax* stability, although in some cases with smaller energy differences (*e.g.*, ΔE(DFT-PBE0/cc-pvdz) = −0.62 kcal mol^{-1}; ΔE(DFT-LDA/cc-pvdz) = −3.1 kcal mol^{-1}). There is a significant difference between the PBE0 functional and simple LDA, implying that treatment of exact electronic exchange is important and that there is likely a large correction for self-interaction. Also, the B3LYP functional, another hybrid functional that includes a small amount of exact exchange, actually finds **3**-*eq* to be more stable (*e.g.*, ΔE(DFT-B3LYP/cc-pvdz) = 0.11 kcal mol^{-1}), although modestly so. Correction for the self-interaction error, implicit in DFT calculations and particularly large for strongly correlated systems, gives **3**-*eq* as the more stable isomer (*e.g.*, ΔE(SICDFT-PBE0/6-311G**) = 4.5 kcal mol^{-1}; ΔE(SICDFT-B3LYP/6-311G**) = 6.1 kcal mol^{-1}). Clearly these systems require a very high level of theory to account for the strong electron correlation effects that are fundamental to the relative stabilities of the two structures.

We also explored full configuration interactions on a restricted active space (CASSCF) and coupled cluster theory that included up to perturbative triples excitations. For the CASSCF(orbitals, electrons) calculations we used an active space of 10 orbitals (5 OMOs and 5 UMOs) and 10 electrons. This relatively small active space, 63 504 determinants, is nonetheless adequate to include both the donor (N lone pair) and acceptor (carbonyl antibonding orbital) portions of the piperidones. The CASSCF(10,10) results find **3**-*eq* as the most stable epimer (*e.g.*, ΔE(CASSCF(10,10)/6-31G*) = 3.0 kcal mol^{-1}). A slightly larger active space (12 orbitals and 12 electrons) lowers the energy difference to 2.3 kcal mol^{-1}.

Finally, there is a substantial difference in the energies when coupled cluster calculations are used (*e.g.*, ΔE(CCSD/STO-3G) = 1.1 kcal mol^{-1}; ΔE(CCSD(T)/STO-3G) = 0.6 kcal mol^{-1}). Larger basis sets (such as the 3-21G or cc-pvdz) lead to a slight preference for **3**-*ax*. The largest basis set that yielded converged results at the CCSD and CCSD(T) levels was cc-pvdz, which gave ΔE(CCSD/cc-pvdz) = −0.36 kcal mol^{-1} and ΔE(CCSD/cc-pvdz) = −1.3 kcal mol^{-1}. The energy differences obtained from coupled cluster, PBE0, and B3LYP calculations are, on average, coincidentally consistent with the solid-state epimer ratio of ~2–3 : 1 *eq* : *ax* (~0.4–0.65 kcal mol^{-1} preference for **3**-*eq*). In the absence of a solution-phase experimental value for the energy difference between **3**-*ax* and **3**-*eq*, it is difficult to determine which method performs best for these systems, independent of basis set. Apparent is that the use of methods that account for strong electron correlation is important,[10a] and each, in general, predicts a significant stability for **3**-*ax*.

The energy-minimized structures of **3**-*ax* and **3**-*eq* do bear resemblance to those found in the solid state, although this need not be the case. An overlay between the calculated (dark gray), at the MP2/cc-pvdz level, and experimentally-determined (light gray) **3**-*eq* structures is shown in Fig. 5(a). The twist angle about the N–C(phenyl) bond is slightly diminished in the calculated structure, by ~10° (to 25.8°), and the nitrogen atom is also slightly flattened by 2° ($\sum_{CNC}$ = 340°). The excellent agreement nonetheless suggests that **3**-*eq* is able to nicely optimize intermolecular and intramolecular interactions in the solid state. A similar analysis with the calculated and experimental structures of **3**-*ax* is inherently less reliable (due to disorder). While the nitrogen is modestly less flattened in the calculated structure (by 8°; $\sum_{CNC}$ = 340°), the N–C(phenyl) twist angle is now ~0° (optimizing interaction between the N lone pair and phenyl ring; this is also shown by NBO calculations, *vide infra*). Along the same lines, it is important to note that subtle differences in the *N*-Ph *ax* configuration do exist among the calculated structures reported in Tables 4 and 5. Even so, the $\sum_{CNC}$ values are consistently 340–343° and the N–C(phenyl) twist angles lie between 0 and 26°.

In order to rationalize, in part, the origin of the **3**-*ax* stability, we performed a natural bond order (NBO) analysis based on the optimized wavefunctions (MP2/cc-pvdz) of the

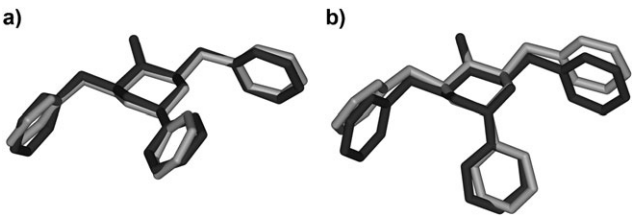

Fig. 5 Superimposed calculated (dark gray; at the MP2/cc-pvdz level) and experimentally-observed (light gray; X-ray) structures for **3**-*eq* (a) and **3**-*ax* (b).

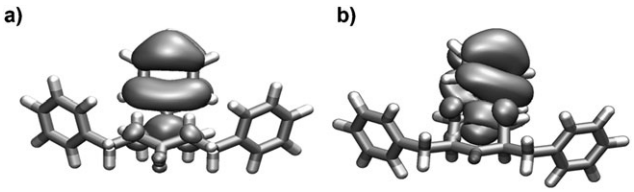

Fig. 6 Plot of the HOMO for **3**-*ax* (a) and **3**-*eq* (b) (energy-minimized structures at the MP2/cc-pvdz level). Delocalization of the nitrogen lone pair into the phenyl ring, adjacent C–C bonds of the piperidone ring, and the carbonyl is observed for **3**-*ax*.

two epimers. This technique is among the best to probe hyperconjugative interactions in molecular systems.[8h,23b,27] The results show, for **3**-*ax*, that the largest second-order stabilization energy (a measure of the degree of hyperconjugation) is due to the delocalization of the N lone pair (donor) orbital into one of the adjacent aromatic C=C π* orbitals (33.52 kcal mol^{-1}). There is also another relatively large stabilization, 8.61 kcal mol^{-1}, due to the N lone pair orbital delocalized into the two σ* C–C orbitals within the piperidone ring. Additionally, and significantly, one of the principle orbital delocalizations for the lone pair is into the π* orbital of the carbonyl group. A plot of the HOMO of the axial epimer shows these delocalizations (Fig. 6(a)). For **3**-*eq*, one main source of stabilization is also from donation of the N lone pair into adjacent aromatic C=C π* orbitals (23.23 kcal mol^{-1}); stabilization from N donation into the two π* C–C orbitals is a comparatively lower 2.34 kcal mol^{-1}. Most importantly, there is no notable delocalization of the N lone pair into the π* orbital of the carbonyl group of **3**-*eq* (Fig. 6(b)). The bond lengths within the calculated structures parallel these findings, where the C(2)–C(3) and C(5)–C(6) bonds in **3**-*ax* (1.547 Å) are somewhat longer than those in **3**-eq (1.536 Å). The trend is in fact detectable throughout the calculated structures when the carbonyl acceptor group is present (*i.e.*, **2**, **7** and **9**), but falls off in its absence (*i.e.*, **6**, **8**, **10** and **11**).

Conclusions

Simple 3,5-disubstituted piperidones have been used to explore donor–acceptor through-bond interactions in the context of molecular and solid-state (supramolecular) assembly structure. The crystal structure of *cis*-3,5-dibenzyl-1-phenylpiperidin-4-one **3** is disordered and the lattice reflects a ~ 3 : 1 mixture of the *N*-Ph equatorial (**3**-*eq*) and *N*-Ph axial (**3**-*ax*) epimers, based on refined values of occupancy factors. The fortuitous result has inspired a side-by-side comparison of the two configurations with respect to their donor–acceptor through-bond interactions. The energy difference between **3**-*ax* and **3**-*eq* has been evaluated in the gas phase using extensive first principles calculations, and for many levels of theory this difference parallels the experimentally-observed configurational ratio in the solid state (where the epimers share nearly identical packing environments). The calculations further show a difference in the relative through-bond stabilization for **3**-*ax* and **3**-*eq*, with larger contributions for **3**-*ax*.[8h] Natural bond order (NBO) analysis quantifies the participation of the piperidone nitrogen and carbonyl groups in stabilization of the **3**-*ax* epimer.

Two important conclusions emerge from the studies. First, the axial/equatorial ratio with respect to the nitrogen substituent in simple piperidones is easily perturbed by the nature of the nitrogen (*e.g.* methyl *vs.* phenyl) *and* ring substituents. It follows that it is particularly inappropriate to employ classic cyclohexane ring substituent parameters to rationalize the piperidine/-one results where "sterics" are outweighed by electronic and stereoelectronic effects. Second, it is reasonable to assume that molecular-level structural perturbations that arise from *or otherwise influence* through-bond donor–acceptor interactions should have a consequence on solid-state assembly structure. Future studies will continue to explore these interactions in the solution phase where they might influence the reversible assembly of molecules.

Experimental

Materials and general methods

Reagents and solvents were purchased from commercial sources and used without further purification unless otherwise specified. THF, ether, CH_2Cl_2, and DMF were degassed in 20 L drums and passed through two sequential purification columns (activated alumina; molecular sieves for DMF) under a positive argon atmosphere. Thin layer chromatography (TLC) was performed on SiO_2-60 F_{254} aluminum plates with visualization by UV light or staining. Flash column chromatography was performed using Purasil SiO_2-60, 230–400 mesh from Whatman. Melting points (mp) were determined on a Mel-temp electrothermal melting point apparatus and are uncorrected. ^1H (^{13}C) NMR spectra were recorded at 300 (75) MHz on Varian Mercury 300, Gemini 300, or VXR 300 spectrometers. Chemical shifts (δ) are given in parts per million (ppm) relative to TMS and referenced to residual protonated solvent ($CDCl_3$: δ_H 7.27 ppm, δ_C 77.00 ppm; toluene-d_8: δ_H 2.09 ppm). Abbreviations used may include s (singlet), d (doublet), t (triplet), q (quartet), quin (quintet), hp (heptet), br (broad) and m (multiplet). UV/Vis absorption spectra were obtained using a Cary 100 Bio spectrophotometer and 1 cm quartz cells. ESI-MS spectra were recorded on a Bruker APEX II FTICR spectrometer. EI-MS spectra were recorded on a Thermo Trace GC DSQ (single quadrupole) spectrometer.

Syntheses

(3*E*,5*E*)-3,5-Dibenzylidene-1-phenylpiperidin-4-one (5b). Benzaldehyde (3.6 mL, 36 mmol) was added to 1-phenylpiperidin-4-one **4b**[11] (3.09 g, 17.6 mmol) under argon protection. Ytterbium triflate (55 mg, 0.088 mmol) was added and the mixture was then heated to 90 °C for 20 h. The mixture was purified by silica gel column chromatography (hexane–EtOAc, 6 : 1) to yield **5b** (2.7 g, 45%) as a yellow solid (Found: C, 85.09; H, 5.99; N, 3.92. $C_{25}H_{21}NO$ requires C, 85.44; H, 6.02; N, 3.99%); mp 160–162 °C; δ_H (300 MHz; $CDCl_3$) 4.63 (s, 4H), 6.68 (d, J = 7.8 Hz, 2H), 6.79 (t, J = 7.2 Hz, 1H), 7.13 (t, J = 7.2 Hz, 2H), 7.45 (m, 10H), 7.90 (s, 2H); δ_C (75 MHz, $CDCl_3$) 51.4, 116.7, 120.2, 128.7, 128.9, 129.2, 130.3, 133.0, 135.0, 137.6, 148.8, 187.2; m/z (EI) 351.1610 (M^+; $C_{25}H_{21}NO$ requires 351.1623).

***cis*-3,5-Dibenzyl-1-methylpiperidin-4-one (2).** (3*E*,5*E*)-3,5-Dibenzylidene-1-methylpiperidin-4-one **5a**[12a] (3.0 g, 10 mmol) in ethanol (100 mL) was hydrogenated (60 psi H_2, 240 mg of 10% palladium on carbon). After being stirred for 36 h at room temperature, the catalyst was filtered off, the solvent was evaporated, and the mixture was purified by column chromatography (hexane–EtOAc, 4 : 1). The desired *cis* diastereomer eluted from the column first (1.7 g, 58%) followed by the *trans* diastereomer (0.16 g, 5%); both were isolated as pale yellow solids. The calculated *d.e.* of *cis*-**2** is 83% based on isolated mass. Single crystals of *cis*-**2** suitable for X-ray analysis were obtained by recrystallization from ethyl ether. For *cis*-**2** (Found: C, 82.12; H, 4.81; N, 8.12. $C_{20}H_{23}NO$ requires C, 81.87; H, 4.77; N, 7.90%); mp 68–69 °C; δ_H (300 MHz; $CDCl_3$) 2.05 (t, J = 8.7 Hz, 2H), 2.24 (s, 3H), 2.40 (dd, J = 11.1, 14.4 Hz, 2H), 2.97 (m, 4H), 3.25 (dd, J = 4.1, 14.1 Hz, 2H), 7.22 (m, 10H); δ_C (75 MHz, $CDCl_3$) 33.2, 45.4, 51.3, 62.3, 126.5, 128.7, 128.8, 129.3, 140.0, 147.5, 210.4; m/z (ESI) 294.1858 ($[M + H]^+$; $C_{20}H_{24}NO$ requires 294.1852). For *trans*-**2**; δ_H (300 MHz; $CDCl_3$) 2.25 (s, 3H), 2.41 (dd, J = 6.3, 11.4 Hz, 2H), 2.62 (dd, J = 4.8, 11.4 Hz, 2H), 2.75 (t, J = 13.2, 2H), 2.86 (m, 2H), 3.15 (dd, J = 4.5, 13.2 Hz, 2H), 7.24 (m, 10H); δ_C (75 MHz, $CDCl_3$) 22.3, 35.3, 45.9, 50.7, 60.3, 126.6, 128.7 129.4, 139.6, 212.3; m/z (ESI) 294.1829 ($[M + H]^+$; $C_{20}H_{24}NO$ requires 294.1852).

***cis*-3,5-Dibenzyl-1-phenylpiperidin-4-one (3).** (3*E*,5*E*)-3,5-Dibenzylidene-1-phenylpiperidin-4-one **5b** (1.8 g, 5.2 mmol) was hydrogenated as described for **2** (60 psi H_2, 150 mg 10% palladium on carbon) to afford **3** (0.75 g, 41%) as a pale yellow solid and a mixture of *cis* and *trans* diastereomers (80% *d.e.* by ^{1}H NMR integration) that could not be separated by column chromatography. Single crystals of *cis*-**3** suitable for X-ray analysis were obtained by recrystallization from diethyl ether (Found: C, 84.19; H, 7.36; N, 3.88. $C_{25}H_{25}NO$ requires C, 84.47; H, 7.09; N, 3.94%); mp 80–81 °C; δ_H (300 MHz; toluene-d_8) 2.34 (dd, J = 8.4, 14.1 Hz, 2H), 2.46 (dd, J = 11.4, 12.1 Hz, 2H), 2.54 (dddd, J = 4.5, 4.8, 8.4, 12.1 Hz, 2H), 3.23 (dd, J = 4.5, 14.1 Hz, 2H), 3.66 (dd, J = 4.8, 11.4 Hz, 2H), 6.49 (m, 2H), 6.67 (m, 1H), 6.98 (m, 2H); δ_C (75 MHz, $CDCl_3$) 32.8, 50.8, 55.3, 115.5, 119.9, 126.6, 128.8, 129.1, 129.2, 129.6, 139.7, 148.6, 209.9; m/z (EI) 355.1938 (M^+; $C_{25}H_{25}NO$ requires 355.1936).

X-Ray crystal structure determination and refinement. Data were collected at 173 K on a Siemens SMART PLATFORM equipped with a CCD area detector and a graphite monochromator utilizing Mo-Kα radiation (λ = 0.71073 Å). Cell parameters were refined using up to 8192 reflections. A full sphere of data (1850 frames) was collected using the ω-scan method (0.3° frame width). The first 50 frames were remeasured at the end of data collection to monitor instrument and crystal stability (maximum correction on I was <1%). Absorption corrections by integration were applied based on measured indexed crystal faces. The structure was solved by the Direct Methods in SHELXTL6,[28] and refined using full-matrix least squares on F^2. The non-H atoms were treated anisotropically, whereas the hydrogen atoms were calculated in ideal positions and were riding on their respective carbon atoms. Details are provided in Table 6. For **3**, the central six-membered ring and the phenyl ring bonded to N(1) are disordered whereas the rest of the molecule falls in the same positions. The disorder was refined in two parts with the site occupancy factors dependently refined. The major part [occupancy factor = 0.76(1)] corresponds to **3**-*eq*; the minor part [occupancy factor = 0.24(1)] corresponds to **3**-*ax*.

CCDC reference numbers 686114 (**2**) and 686115 (**3**).

For crystallographic data in CIF or other electronic format see DOI: 10.1039/b808818g

Computational methods. The fundamental properties and equilibrium structures of the axial and equatorial epimers of the *N*-substituted piperidines/-ones were examined using extensive first principles calculations based on quantum many-body theory (*via* many body perturbation theory (MBPT), coupled clusters (CC), and configuration interactions (CI) on a defined active space) and density functional theory (DFT). All-electron calculations were performed at each level of theory using the NWChem package.[29] For the DFT calculations, both the local density (LDA) and generalized gradient approximations (GGA) were employed. However, in general, the available functionals that can be used in DFT calculations of materials properties suffer from the self-interaction of the electrons that stems from incomplete cancellation between self-interaction in the Coulomb interaction and in the exchange interaction. A framework for the self-consistent calculation of self-interaction corrections (SIC) to the density functional theory (DFT) based on the original method of Perdew and Zunger[30] can be implemented based on a number of variants. One approach, a perturbation treatment, uses the Kohn–Sham orbitals determined from the self-consistent calculations and performs orbital localization with the Foster-Boys algorithm.[31] The self-interaction energy is added to the total energy. The advantage of this approach is that all exchange–correlation functionals implemented in NWChem can be used with this option. We employ this approach in the present study but have also considered the more accurate treatment of SIC using the optimized effective potential (OEP). For the many body quantum calculations, these included at the simplest level Møller–Plesset second order perturbation theory (MP2).[32] MP2 can typically account (depending on the basis set) for up to 90% of the electron correlation energy and is among the most efficient methods for including such effects. In order to investigate higher order and non-dynamical correlation effects we used configuration interaction calculations on a restricted space (CASSCF).[33] Additionally, higher level calculations based on coupled cluster calculations that included singles, doubles and perturbative triples, CCSD(T), were carried out.

For all calculations, we have used atom centered, contracted Gaussian basis sets, ranging from the Pople split-valence basis sets (*i.e.*, 6-31G*, 6-311G**, *etc.*)[34] to the Dunning correlation consistent basis sets (cc-pVXZ and aug-cc-pVXZ)[35] during the calculation of the self-consistent solution. In all cases, full geometry optimization was performed for each epimer. Tight convergence criteria were used for the MP2 calculations: Convergence for the SCF was 10^{-8}, the AO and MO integrals

Table 6 Crystallographic data and processing parameters for *cis*-3,5-dibenzylpiperidin-4-one derivatives **2** and **3**. For the methods used in the structure determination, see the experimental section[a]

	2	**3**
Formula	$C_{20}H_{23}NO$	$C_{25}H_{25}NO$
M_r	293.39	355.46
T/K	173(2)	173(2)
λ/Å	0.71073	0.71073
Crystal system	Monoclinic	Monoclinic
Space group	$P2_1/n$	$P2_1/n$
a/Å	9.5059(7)	15.1125(12)
b/Å	12.3970(9)	5.5285(4)
c/Å	14.7096(11)	23.3378(18)
β/°	102.928(2)	91.899(2)
V/Å^3	1689.5(2)	1948.8(3)
Z	4	4
D_c/g cm^{-3}	1.153	1.212
μ/mm^{-1}	0.070	0.073
$F(000)$	632	760
Crystal size/mm	0.25 × 0.23 × 0.11	0.30 × 0.21 × 0.18
θ range/°	2.17–27.50	1.58–27.50
Reflections collected	10 768	12 085
Independent reflections	3786 (R_{int} = 0.0427)	4385 (R_{int} = 0.0315)
Observed reflections ($I > 2\sigma(I)$)	2040	2662
Parameters	199	285
Goodness-of-fit on F^2	0.786	0.919
Final R indices	R_1 = 0.0331,[a] wR_2 = 0.0661[b]	R_1 = 0.0379,[a] wR_2 = 0.0890[b]
$\Delta\rho$ (max., min.)/e Å^{-3}	0.115, –0.143	0.115, –0.157

[a] $R_1 = \sum(||F_o| - |F_c||)/\sum|F_o|$. [b] $wR_2 = [\sum[w(F_o^2 - F_c^2)^2]/\sum[w(F_o^2)^2]]^{1/2}$; $w = 1/[\sigma^2(F_o^2) + (mp)^2 + np]$; $p = [\max(F_o^2,0) + 2F_c^2]/3$, m and n are constants.

10^{-11}, and the CPHF 10^{-5}; energy convergence for the geometry optimization was 10^{-7} with a maximum gradient of 10^{-5}. For compounds **2** and **10** of Table 4, this level of convergence was not reached on the geometry optimization. For **2**-*ax*, the energy convergence was to 6.8×10^{-6} (max grad = 2.7×10^{-4}); for **2**-*eq*, the energy convergence was to 1.8×10^{-5} (max grad. = 1.7×10^{-4}). Likewise, for compound **10**: **10**-*ax* energy convergence to 3.8×10^{-5} (max grad. = 1.1×10^{-3}); **10**-*eq* energy convergence to 1.7×10^{-6} (max grad = 7.1×10^{-4}). For the DFT, CASSCF, and coupled cluster calculations, the NWChem default tolerances were used.

The electronic structure of **3** was probed by the natural bond orbital (NBO) method of Weinhold and co-workers.[36] This method uses the one electron density matrix to define the shape of the atomic orbitals in the molecular environment, and to derive molecular bonds from the density between atoms. In short, the optimized wavefunction at a given level of theory is localized to obtain canonical molecular orbitals that are transformed into an orthonormal set of localized NBOs. In this representation, formal core orbitals, σ and π orbitals (both bonding and antibonding), lone pairs and Rydberg orbitals are explicitly given and it also permits the assignment of hybridization both to the atomic lone pairs and to each atom's contributions to its bond orbitals. Since the NBOs do not diagonalize the Fock or Kohn–Sham operator, off-diagonal elements will be non-zero and second-order perturbation theory has shown that these off-diagonal elements give an energy that is directly related to the stabilization energy due to that interaction. In the present study, the stabilization energy resulting from the interactions of the electron lone pair on the nitrogen with other orbitals on the molecule was evaluated and the influence of through-bond interactions quantified.

Acknowledgements

This work was financially supported by the National Science Foundation CAREER program (CHE-0548003) and the University of Florida. B. G. S. thanks the Center for Nanophase Materials Sciences (CNMS), sponsored by the Division of Scientific User Facilities, US Department of Energy. The extensive computations were performed using the resources of the National Center for Computational Sciences at Oak Ridge National Laboratories (ORNL). R. K. C. is grateful to the CNMS User Program (CNMS2004-016 and CNMS2007-029) for resources. K. A. A. thanks the National Science Foundation and University of Florida for funding the X-ray crystallography equipment. We are additionally grateful to Juergen Koeller for his assistance with processing the X-ray data, Dr Ion Ghiviriga for help obtaining the ^{1}H NMR spectra of **2** and **3**, and Dr Edo Apra for useful discussions and help with the CCSD(T) calculations.

References

1 (*a*) N. Risch, *J. Chem. Soc., Chem. Commun.*, 1983, 532–533; (*b*) A. J. Lampkins, Y. Li, A. Al Abbas, K. A. Abboud, I. Ghiviriga and R. K. Castellano, *Chem. Eur. J.*, 2008, **14**, 1452–1463.
2 (*a*) R. Hoffmann, A. Imamura and W. J. Hehre, *J. Am. Chem. Soc.*, 1968, **90**, 1499–1509; (*b*) R. Hoffmann, *Acc. Chem. Res.*, 1971, **4**, 1–9; (*c*) R. Gleiter, W. D. Stohrer and R. Hoffmann, *Helv. Chim. Acta*, 1972, **55**, 893–906; (*d*) R. Gleiter, *Angew. Chem., Int. Ed. Engl.*, 1974, **13**, 696–701; (*e*) M. N. Paddon-Row, *Acc. Chem. Res.*, 1982, **15**, 245–251; (*f*) R. Gleiter and W. Schafer, *Acc. Chem. Res.*, 1990, **23**, 369–375.
3 (*a*) J. B. Lambert, Y. Zhao, R. W. Emblidge, L. A. Salvador, X. Liu, J.-H. So and E. C. Chelius, *Acc. Chem. Res.*, 1999, **32**, 183–190; (*b*) I. V. Alabugin and T. A. Zeidan, *J. Am. Chem. Soc.*, 2002, **124**, 3175–3185; (*c*) I. V. Alabugin and M. Manoharan, *J. Org. Chem.*, 2004, **69**, 9011–9024.

4 (*a*) R. C. Cookson, J. Henstock and J. Hudec, *J. Am. Chem. Soc.*, 1966, **88**, 1060–1062; (*b*) R. C. Cookson, *Proc. R. Soc. London Ser. A*, 1967, **297**, 27–39.
5 J.-M. Lehn, *Supramolecular Chemistry*, VCH, Weinheim, 1995.
6 (*a*) H. Li, E. A. Homan, A. J. Lampkins, I. Ghiviriga and R. K. Castellano, *Org. Lett.*, 2005, **7**, 443–446; (*b*) A. J. Lampkins, O. Abdul-Rahim, H. Li and R. K. Castellano, *Org. Lett.*, 2005, **7**, 4471–4474; (*c*) B. G. Sumpter, V. Meunier, Á. Vázquez-Mayagoitia and R. K. Castellano, *Int. J. Quantum Chem.*, 2007, **107**, 2233–2242.
7 B. G. Sumpter, V. Meunier, E. F. Valeev, A. J. Lampkins, H. Li and R. K. Castellano, *J. Phys. Chem. C*, 2007, **111**, 18912–18916.
8 (*a*) A. W. J. Dekkers, J. W. Verhoeven and W. N. Speckamp, *Tetrahedron*, 1973, **29**, 1691–1696; (*b*) P. Pasman, J. W. Verhoeven and T. J. de Boer, *Tetrahedron*, 1976, **32**, 2827–2830; (*c*) A. M. Halpern and A. L. Lyons, *J. Am. Chem. Soc.*, 1976, **98**, 3242–3247; (*d*) G. Spanka and P. Rademacher, *J. Org. Chem.*, 1986, **51**, 592–596; (*e*) B. Krijnen, H. B. Beverloo and J. W. Verhoeven, *Recl. Trav. Chim. Pays-Bas.*, 1987, **106**, 135–136; (*f*) B. Krijnen, H. B. Beverloo, J. W. Verhoeven, C. A. Reiss, K. Goubitz and D. Heijdenrijk, *J. Am. Chem. Soc.*, 1989, **111**, 4433–4440; (*g*) T. Scherer, W. Hielkema, B. Krijnen, R. M. Hermant, C. Eijckelhoff, F. Kerkhof, A. K. F. Ng, R. Verleg, E. B. van der Tol, A. M. Brouwer and J. W. Verhoeven, *Recl. Trav. Chim. Pays-Bas*, 1993, **112**, 535–548; (*h*) W. D. Oosterbaan, R. W. A. Havenith, C. A. van Walree, L. W. Jenneskens, R. Gleiter, H. Kooijman and A. L. Spek, *J. Chem. Soc., Perkin Trans. 2*, 2001, 1066–1074; (*i*) D. J. A. De Ridder, K. Goubitz, H. Schenk, B. Krijnen and J. W. Verhoeven, *Helv. Chim. Acta*, 2003, **86**, 799–811; (*j*) D. J. A. De Ridder, K. Goubitz, H. Schenk, B. Krijnen and J. W. Verhoeven, *Helv. Chim. Acta*, 2003, **86**, 812–826.
9 (*a*) M. Rubiralta, E. Giralt and A. Díez, *Piperidine. Structure, Preparation, Reactivity and Synthetic Applications of Piperidine and its Derivatives*, Elsevier, Amsterdam, 1991; (*b*) W. Schuddeboom, B. Krijnen, J. W. Verhoeven, E. G. J. Staring, G. Rikken and H. Oevering, *Chem. Phys. Lett.*, 1991, **179**, 73–78; (*c*) K. Srinivas, S. Sitha, V. J. Rao, K. Bhanuprakash, K. Ravikumar, S. P. Anthony and T. P. Radhakrishnan, *J. Mater. Chem.*, 2005, **15**, 965–973.
10 (*a*) A. M. Brouwer and B. Krijnen, *J. Org. Chem.*, 1995, **60**, 32–40; (*b*) K. Ogawa, J. Harada, M. Endo, Y. Takeuchi and H. Kagawa, *Tetrahedron Lett.*, 1997, **38**, 5663–5666.
11 D. R. Tortolani and M. A. Poss, *Org. Lett.*, 1999, **1**, 1261–1262.
12 (*a*) S. M. McElvain and K. Rorig, *J. Am. Chem. Soc.*, 1948, **70**, 1820–1825; (*b*) S. Z. Vatsadze, M. A. Manaenkova, N. V. Sviridenkova, N. V. Zyk, D. P. Krut'ko, A. V. Churakov, M. Yu. Antipin, J. A. K. Howard and H. Lang, *Russ. Chem. Bull.*, 2006, **55**, 1184–1194.
13 L. Wang, J. Sheng, H. Tian and C. Qian, *Synth. Commun.*, 2004, **34**, 4265–4272.
14 H. I. El-Subbagh, S. M. Abu-Zaid, M. A. Mahran, F. A. Badria and A. M. Al-Obaid, *J. Med. Chem.*, 2000, **43**, 2915–2921.
15 M. D. Brown, M. J. Cook, G. Desimoni and A. R. Katritzky, *Tetrahedron*, 1970, **26**, 5281–5287.
16 (*a*) E. A. Meyer, R. K. Castellano and F. Diederich, *Angew. Chem., Int. Ed.*, 2003, **42**, 1210–1250; (*b*) M. Nishio, *CrystEngComm*, 2004, **6**, 130–158.
17 (*a*) A. Bouchemma, P. H. McCabe and G. A. Sim, *J. Chem. Soc., Perkin Trans. 2*, 1989, 583–587; (*b*) A. Bouchemma, P. H. McCabe and G. A. Sim, *Acta Crystallogr., Sect. C*, 1988, **44**, 1469–1472; (*c*) A. Bouchemma, P. H. McCabe and G. A. Sim, *Acta Crystallogr., Sect. C*, 1990, **46**, 410–414; (*d*) A. Bouchemma, P. H. McCabe and G. A. Sim, *Acta Crystallogr., Sect. C*, 1990, **46**, 671–674; (*e*) A. Bouchemma, P. H. McCabe and G. A. Sim, *Acta Crystallogr., Sect. C*, 1991, **47**, 1219–1222; (*f*) D. Adam, P. H. McCabe, G. A. Sim and A. Bouchemma, *Acta Crystallogr., Sect. C*, 1993, **49**, 837–841; (*g*) D. Adam, P. H. McCabe, G. A. Sim and A. Bouchemma, *Acta Crystallogr., Sect. C*, 1995, **51**, 246–249; (*h*) R. Glaser, I. Adin, D. Shiftan, Q. Shi, H. M. Deutsch, C. George, K.-M. Wu and M. Froimowitz, *J. Org. Chem.*, 1998, **63**, 1785–1794; (*i*) R. Glaser, A. Novoselsky, D. Shiftan and M. Drouin, *J. Org. Chem.*, 2000, **65**, 6345–6353.
18 R. K. Castellano, *Curr. Org. Chem.*, 2004, **8**, 845–865.
19 M. D. Rozeboom, K. N. Houk, S. Searles and S. E. Seyedrezai, *J. Am. Chem. Soc.*, 1982, **104**, 3448–3453.
20 All of the proton chemical shifts of the piperidone core respond to solvent polarity; only H_d and H_e remain essentially constant.
21 (*a*) P. J. Crowley, M. J. T. Robinson and M. G. Ward, *Tetrahedron*, 1977, **33**, 915–925; (*b*) A. R. Katritzky, R. C. Patel and F. G. Riddell, *Angew. Chem., Int. Ed. Engl.*, 1981, **20**, 521–529; (*c*) T. A. Crabb and A. R. Katritzky, *Adv. Heterocycl. Chem.*, 1984, **36**, 1–173.
22 (*a*) M. Bixon, H. Dekker, J. D. Dunitz, H. Eser, S. Lifson, C. Mosselma, J. Sicher and M. Svoboda, *Chem. Commun.*, 1967, 360–362; (*b*) G. I. Birnbaum, G. W. Buchanan and F. G. Morin, *J. Am. Chem. Soc.*, 1977, **99**, 6652–6656; (*c*) G. A. Sim, *J. Chem. Soc., Chem. Commun.*, 1987, 1118–1120; (*d*) E. Alessio, E. Zangrando, R. Roppa and L. G. Marzilli, *Inorg. Chem.*, 1998, **37**, 2458–2463; (*e*) K. Ananda, S. Aravinda, P. G. Vasudev, K. Muruga Poopathi Raja, H. Sivaramakrishnan, K. Nagarajan, N. Shamala and P. Balaram, *Curr. Sci.*, 2003, **85**, 1002–1011.
23 (*a*) G. R. Desiraju, *Angew. Chem., Int. Ed.*, 2007, **46**, 2–17; (*b*) I. V. Alabugin, M. Manoharan, M. Buck and R. J. Clark, *THEOCHEM*, 2007, **813**, 21–27.
24 M. J. T. Robinson, *J. Chem. Soc., Chem. Commun.*, 1975, 844–845.
25 (*a*) M. Aroney and R. J. W. Le Fèvre, *J. Chem. Soc.*, 1960, 2161–2168; (*b*) S. F. Beach, J. D. Hepworth, J. Sawyer, G. Hallas, R. Marsden, M. M. Mitchell, D. A. Ibbitson, A. M. Jones and G. T. Neal, *J. Chem. Soc., Perkin Trans. 2*, 1984, 217–221.
26 E. Kleinpeter, *Adv. Heterocycl. Chem.*, 2004, **86**, 41–127.
27 I. V. Alabugin, *J. Org. Chem.*, 2000, **65**, 3910–3919.
28 SHELXTL6, Bruker-AXS, Madison, WI, USA, 2000.
29 R. A. Kendall, E. Aprà, D. E. Bernholdt, E. J. Bylaska, M. Dupuis, G. I. Fann, R. J. Harrison, J. Ju, J. A. Nichols, J. Nieplocha, T. P. Straatsma, T. L. Windus and A. T. Wong, *Comput. Phys. Commun.*, 2000, **128**, 260–283.
30 J. P. Perdew and A. Zunger, *Phys. Rev. B*, 1981, **23**, 5048–5079.
31 J. M. Foster and S. F. Boys, *Rev. Mod. Phys.*, 1960, **32**, 300–302.
32 Chr. Møller and M. S. Plesset, *Phys. Rev.*, 1934, **46**, 618–622.
33 B. O. Roos and P. R. Taylor, *Chem. Phys.*, 1980, **48**, 157–173.
34 (*a*) W. J. Hehre, R. Ditchfield and J. A. Pople, *J. Chem. Phys.*, 1972, **56**, 2257–2261; (*b*) J. S. Binkley, J. A. Pople and W. J. Hehre, *J. Am. Chem. Soc.*, 1980, **102**, 939–947.
35 (*a*) T. H. Dunning, *J. Chem. Phys.*, 1989, **90**, 1007–1023; (*b*) R. A. Kendall, T. H. Dunning and R. J. Harrison, *J. Chem. Phys.*, 1992, **96**, 6796–6806; (*c*) A. K. Wilson, T. Mourik and T. H. Dunning, *J. Mol. Struct.*, 1996, **388**, 339–349.
36 (*a*) J. P. Foster and F. Weinhold, *J. Am. Chem. Soc.*, 1980, **102**, 7211–7218; (*b*) A. E. Reed, R. B. Weinstock and F. Weinhold, *J. Chem. Phys.*, 1985, **83**, 735–746.

